

Chapter 2

Resonance Properties of Metallic Ring Systems: A Single Ring

2.1 Introduction

In 1968, Veselago proposed that a medium with simultaneously negative permittivity and permeability possesses a negative refractive index, and exhibits many unusual EM properties [1]. This proposal did not attract immediate attention, since it is well accepted that a natural material shows no magnetism at high frequencies [2]. A breakthrough appeared in 1999, when Pendry showed that a split-ring resonator (SRR) could provide magnetic responses at any desired frequency [3]. Metamaterials with negative refractive index were then successfully fabricated by combining SRRs and electric wires [4], and later the concept of metamaterial was greatly expanded to beyond negative-index materials. Many unusual EM phenomena were subsequently demonstrated based on metamaterials, such as negative refraction [4–10], super focusing [11–14], and subwavelength resonant cavities [15–17].

As the first realization of artificial magnetism, the SRR structures naturally attracted the most extensive attention. Circular SRRs [3, 4, 6, 18–36], rectangular SRRs [5, 37–51], SRRs with different cross-sections, metal line widths, metal thicknesses, and substrates [4–6, 19, 38, 43, 44], SRRs with different numbers of splits [19, 20, 39], and different numbers of rings [31, 47] have been studied. Applications were also proposed for the SRR, for instance, as antennas [52], as couplers for channel dropping [53]. SRRs were inserted inside a cut-off waveguide to enhance the transmission [54, 55], and as a lens for imaging [56, 57]. Recently, the designs and fabrications of isotropic metamaterials began to draw intensive attentions [58–64].

Many theoretical efforts were devoted to understand the exotic EM wave properties of the SRR structures. Pendry et al. [3] first analyzed the resonance properties of a SRR by assuming a metallic ring as a single lumped element with empirical circuit characteristics. Later, Shamonin et al. considered more inductive/capacitive effects by assuming the SRR to consist of an infinite number of lumped circuit elements [25]. Many other analytical methods were developed to study the

properties of SRRs [24, 26–29, 31, 32, 47, 48] from various aspects. However, in all these approaches, the inductive/capacitive effects in the rings were not *completely* considered, since self (mutual)-inductive/capacitive effects exist everywhere inside the system. In addition, all these approaches need a set of empirical circuit parameters that cannot be calculated rigorously. Those empirical parameters were generally determined under some approximations [3, 25]. The SRR systems have also been studied by numerical calculations [37, 38, 44, 45, 49, 50]. Although such full-wave studies contain all relevant field information, it is sometimes difficult to extract useful properties of an SRR, such as the bianisotropy polarizabilities, from the obtained information.

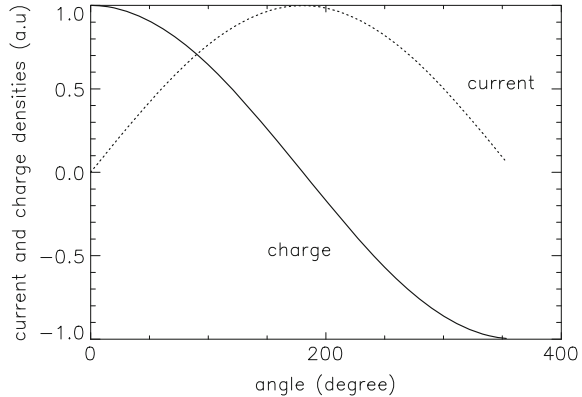
We recently developed an analytical approach on more rigorous ground for metallic wire systems [33–36]. In this chapter, we illustrate our approach to wires in ring geometries, and apply it to quantitatively study the EM resonance properties of a single ring SRR [33]. In our theory, the inductive/capacitive effects are *fully* included and all circuit parameters are calculated *rigorously*. One of the key ideas of our approach is a simple way to implement the boundary condition that the current is zero at the free ends of the wire. This idea consists of the introduction of localized electric fields at ends and junctions. We show that the circuit equations can be analytically solved in the thin-wire limit, leading to useful analytical formulas. Our theoretical results were all successfully verified by FDTD simulations on realistic systems and/or available experiments. This chapter is organized as follows. We describe our simple picture of split rings in the next section, briefly review the theoretical developments in Sects. 2.3 and 2.4, and then apply our theory to study the EM resonance properties of a single ring SRR analytically (Sect. 2.5) and numerically (Sect. 2.6). For those readers who prefer to go directly to the heart of the matter, they can start with Eq. (2.18) where the circuit equation in the angular momentum basis including the localized field is introduced. We summarize our results in the last section.

2.2 Simple Physical Picture

Before we start going into the details of dealing with the problem quantitatively, first we would like to explain the simple physics for this class of structures. Central to the understanding of the EM response is the resonance mode of a wire structure. These resonance modes are characterized by the spatial dependence of the tangential current along the wire. To a good approximation the current depends on the *arc length* of the wire sinusoidally with a period that is twice the length of the wire divided by an integer. This is independent of the shape of the wire. The more spatial oscillation the current exhibits, the higher the resonance frequency of the normal mode. We shall see why this is true and how this will be modified quantitatively when the wire becomes thicker.

From this spatial dependence of the current one can calculate the response of the wire to external EM fields. The response is characterized by the multipole

Fig. 2.1 The current and charge densities as a function of angle for the lowest resonance of a single ring SRR



moments induced. Because different wire structures can have different shapes, the multipole moments will depend on the shape of the wire structure. The magnetic moments depend on the current and can be easily calculated. For example, for the split ring we get a finite magnetic moment, whereas for the dipole antenna we do not, even though the normal modes, when expressed in arc length, are very similar. The electric multipole moments can be derived from the charge density ρ , which can be determined from the charge-current conservation law as $\rho = i\nabla \cdot \vec{j}/\omega$. To illustrate, we show in Fig. 2.1 the dependence of the current on the azimuthal angle for the lowest mode of a split ring. Note that the current is zero at the free ends. The corresponding charge density is also shown in Fig. 2.1. For this mode, the electric dipole moment is in the plane of the ring, whereas the magnetic dipole moment is perpendicular to the ring. Either an external electric or magnetic field can excite this normal mode, generating both an electric, and a magnetic moment. This picture remains valid as the number of wires is increased or the topology is changed.

2.3 Circuit Parameters for a Single Ring

We consider a single ring of radius R with a small gap at $\phi = 0^\circ$ lying on the xy -plane, as shown in Fig. 2.2 [33]. In what follows, a common time-varying factor $e^{i\omega t}$ is omitted for every quantity. We assume that $a \ll R$, where a is the radius of the metal wire forming the ring. For a good metal, the skin effect dictates that the current should mainly distribute on the metal surface, within a thin layer of a thickness equal to the metal skin depth $\delta = (\mu\omega\sigma/2)^{-1/2}$. For typical material like Cu with a resistivity $1/\sigma = 1.68 \times 10^{-8} \Omega \cdot m$, we get

$$\delta = 3.76\lambda^{1/2} \mu m \quad (2.0)$$

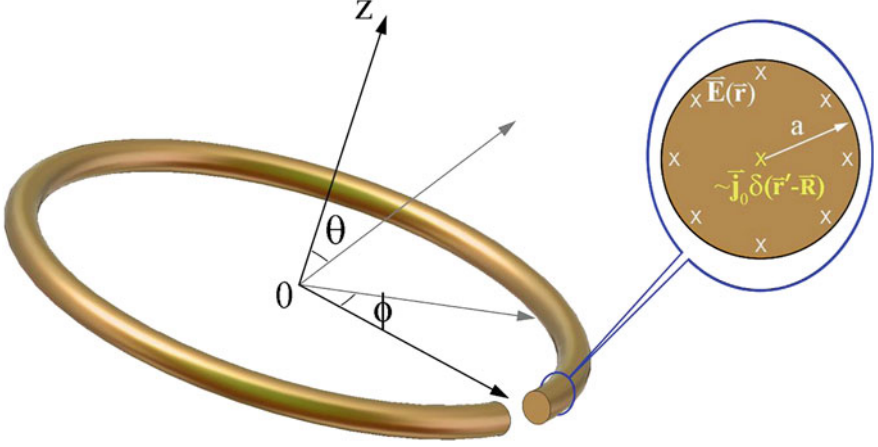


Fig. 2.2 Geometries of a single ring SRR

at a wavelength of λ measured in m. Typically, the largest wavelength of interest is of the order of twice the circumference: $\lambda \approx 4\pi R$ (see below). We thus get $\delta/R \approx 0.47 \times 10^{-4}/\lambda^{1/2}$. From microwave to infrared frequencies with the wavelengths of the order of a centimeter to a micron, the current flows on the conductor's outer surface within a layer of thickness of the order of the skin depth, so that $\vec{j}(\vec{r}')$ is basically a very complicated function of \vec{r}' . However, when the wire is very thin, we can simplify the realistic current distribution as a delta-function localized in the middle of the wire,

$$\vec{j}(\vec{r}') = \vec{e}_{\phi'} I(\phi') \sin \theta' \delta(\cos \theta') \delta(r' - R)/R \quad (2.1)$$

With $\vec{e}_{\phi'} = -\sin \phi' \vec{e}_x + \cos \phi' \vec{e}_y$. This simplification will *not* generate any significant errors for calculating the fields outside the metal wire in the thin-wire limit. On the other hand, both the inductive $\vec{E}_L(\vec{r})$ [Eq. (1.4)] and the capacitive electric fields $\vec{E}_C(\vec{r})$ [Eq. (1.5)] should still be calculated on the outer surface of the metal wire where the current *physically* flows. Again considering the fact $a \ll R$, we understand that $\vec{E}_L(\vec{r})$ and $\vec{E}_C(\vec{r})$ would not vary dramatically around the wire (as long as on the same position of the ring with a fixed ϕ), so that we can pick up a particular (convenient) point on the wire surface to calculate these fields.

The particular symmetry of the ring geometry indicates that all physical quantity (i.e., $I(\phi)$, $\vec{E}_L(\vec{r})$, and $\vec{E}_C(\vec{r})$, etc.) are periodic functions of ϕ with period of 2π . Therefore, we can expand those quantifiers as a Fourier series of the azimuthal angle ϕ . Such a choice of basis will simplify the calculations dramatically, as will be shown soon. Substituting Eq. (2.1) into Eq. (1.4), we can choose a particular observation point on the wire surface to calculate the inductive field *projected along the wire direction*,

$$\vec{E}_L(\phi) \cdot \hat{e}_\phi = -i\omega \int (\hat{e}_\phi \cdot \hat{e}_{\phi'}) I(\phi') g(\phi, \phi') R d\phi' / c^2, \quad (2.2)$$

where the reduced Green's function is defined by

$$g(\phi, \phi') = G(\vec{r}, \vec{r}')|_{r'=R, \theta'=\pi/2; r=R-a, \theta=\pi/2} \quad (2.3)$$

so that r is at the surface and r' is at the center of the wire. Here the observation point is selected at $(r = R - a, \theta = \pi/2, \phi = \phi)$ for the convenience of calculations and $r' = R, \theta' = \pi/2$ come from the fact that current is localized at the wire center. Other choice of observation point will not affect the final results under the thin-wire limit, but the calculations may not be as easy as the present choice.

Putting the Fourier expansion $I(\phi') = \sum_{m=-\infty}^{+\infty} I_m e^{im\phi'}$ into Eq. (2.2), we obtain that

$$E_L^m = -i\omega \sum_{m'} L_{mm'} I_{m'} \quad (2.4)$$

where

$$E_L^m = \frac{1}{2\pi} \int_0^{2\pi} (\vec{E}_L \cdot \vec{e}_\phi) e^{-im\phi} d\phi \quad (2.5)$$

and

$$L_{mm'} = \frac{1}{2\pi c^2} \iint (\hat{e}_\phi \cdot \hat{e}_{\phi'}) e^{i(m'\phi' - m\phi)} g(\phi, \phi') R d\phi' d\phi \quad (2.6)$$

are the elements of the inductance matrix. Similarly, we obtain the result

$$E_C^m = -\frac{1}{i\omega} \sum_{m'} (C^{-1})_{mm'} I_{m'}, \quad (2.7)$$

where

$$E_C^m = \frac{1}{2\pi} \int_0^{2\pi} (\vec{E}_C \cdot \vec{e}_\phi) e^{-im\phi} d\phi \quad (2.8)$$

is the Fourier component of the capacitive field projected along the wire direction, and

$$(C^{-1})_{mm'} = -\frac{1}{2\pi} \iint (im') e^{i(m'\phi' - m\phi)} \frac{1}{(R-a)} \left(\frac{\partial}{\partial \phi} g(\phi, \phi') \right) d\phi' d\phi \quad (2.9)$$

are the capacitance matrix elements. Both the inductance and capacitance matrixes can be calculated numerically by performing the integrations in Eqs. (2.6) and (2.9). For the present symmetric ring geometry, analytical formulas can be derived,

which offer us physical insights. The details of this are described in [Appendix](#) in this chapter. The result under the quasi-static approximation (QSA) contains the leading log contribution and will be discussed here. Corrections beyond the QSA are discussed in the Appendix. Putting the formula ($r_{>}$, $r_{<}$ are the larger and the smaller of r , r')

$$\frac{1}{|\vec{r} - \vec{r}'|} = \sum_{l=0}^{\infty} \sum_{m=-l}^l \frac{4\pi}{2l+1} Y_{lm}(\theta, \phi) Y_{lm}^*(\theta', \phi') \frac{r_{<}^l}{r_{>}^{l+1}} \quad (2.10)$$

into Eqs. (2.6) and (2.3), we find for the present ring geometry that $L_{mm'}$ and $(C^{-1})_{mm'}$ are diagonal with matrix elements given by

$$\begin{aligned} L_{mm'} &= \delta_{mm'} L_m = \delta_{mm'} (A_{m-1} + A_{m+1}) \pi / c^2 \\ (C^{-1})_{mm'} &= \delta_{mm'} (C_m)^{-1} = \delta_{mm'} m^2 A_m 2\pi / [R(R-a)] \end{aligned} \quad (2.11)$$

The function A_m is defined as

$$A_m = \sum_{l=|m|}^{\infty} \frac{(l-m)!}{(l+m)!} \alpha^l [P_l^m(0)]^2 \quad (2.11a)$$

where P_l^m is the associated Legendre function, and $\alpha = (R-a)/R < 1$.

There are several important points about the circuit parameters:

- (1) In the thin-wire limit ($a \ll R$), the sum in Eq. (2.6) can be carried out analytically. We found (see [Appendix](#) in this chapter) an asymptotic form

$$A_m \approx D_m - \ln(2a/R) / (\alpha^m \pi). \quad (2.12)$$

Thus in this limit all the A_m are the same. The inductances are independent of m . We obtain

$$L_m = -2 \ln(2a/R) / c^2. \quad (2.12a)$$

Similarly we get

$$1/C_m = -2m^2 \ln(2a/R) / R^2. \quad (2.12b)$$

This logarithmic divergence is a typical characteristic of a thin-wire system [65]. It comes out because of the factor of $1/|\vec{r} - \vec{r}'|$ in the Green's function inside the integrations for the inductive/capacitive fields. Such logarithmic dependence of circuit parameters on wire radius is the basis to justify for the QSA, as we have discussed in [Chap. 1](#). In wire structures of lower symmetry, the circuit parameters are no longer “diagonal” and we have to consider the “off-diagonal” elements of matrixes L and C^{-1} . As we shall show in the next chapter this off-diagonal element with m not equal to m' is not log divergent and much smaller. Much of computational electromagnetics involves calculating the inverse of the matrix $L_{mm'}$ and/or $(C^{-1})_{mm'}$ in a local basis. In our basis, it is nearly diagonal; the inversion of the

matrixes $L_{mm'}$ and $(C^{-1})_{mm'}$ becomes simpler, the physical implication of the results is much easier to understand.

- (2) In our basis $(C_m)^{-1}$ is proportional to m^2 . Thus I_m , which is of the order of $C_m E_m$, decreases rapidly as m is increased. This sets the limit of the number of Fourier mode that needs to be retained. In the following, to emphasize this point, we sometimes write $(C_m)^{-1}$ as $m^2/\overline{C_m}$.
- (3) One can consider the $m = 0$ components to correspond to the lump circuit elements normally considered. The approach here thus provides for a simple extension of previous considerations. However, there is no $m = 0$ capacitive term. To include a capacitive effect, the $m = 1$ term need to be included.
- (4) If one goes beyond the QSA, a damping term proportional to kR will be introduced in addition to the log divergent terms, as is discussed in the Appendix.

The above characteristics are true for all wire structures and will be exploited in our discussion in later chapters.

2.4 Implementation of the Boundary Conditions

We can now solve the circuit Eq. (1.1)

$$\rho(\vec{r})\vec{j}(\vec{r}, t) = \vec{E}_{\text{ext}}(\vec{r}, t) + \vec{E}_L(\vec{r}, t) + \vec{E}_C(\vec{r}, t).$$

in the basis that we have chosen. So far we have assumed that the Fourier components of the current are independent variables. There is a boundary condition that the current at the gap vanishes, $I(\phi = 0) = 0$, which can be written as $\sum_m I_m = 0$ in terms of the Fourier components. We describe, in this chapter, two ways that we have tried to implement this condition. They lead to identical results, thus providing confidence in our method. We describe these next.

2.4.1 The Gap Resistance Approach

The boundary condition of zero current can be incorporated by introducing a very large resistance in the gap region. In terms of the Fourier components and using the formulas derived in last section, Eq. (1.1) can be written as the following matrix equation,

$$\sum_{m'} H_{mm'} I_{m'} = E_{\text{ext}}^m, \quad (2.13)$$

where

$$H_{mm'} = \bar{\rho}(m - m') + i\omega L_m(1 - \Omega_m^2/\omega^2)\delta_{mm'}. \quad (2.14)$$

Here, $\bar{\rho}(m - m')$ is the Fourier component of the normalized resistivity function defined by $\bar{\rho}(\phi) = \rho(\phi)/S$ (S is the wire cross-section area and $\rho(\phi)$ is the true resistivity function) and $\Omega_m = 1/\sqrt{L_m C_m}$. In the thin-wire limit ($a/R \rightarrow 0$), $\Omega_m \rightarrow m\omega_u$ where

$$\omega_u = c/R \quad (2.14a)$$

is the frequency unit of the present problem. Suppose $\bar{\rho}(\phi) = \bar{\rho}_0$ inside the gap of width Δ centered at $\phi = 0$ and $\bar{\rho}(\phi) = r_c$ elsewhere (in the metallic wire), we found easily that

$$\bar{\rho}(m - m') = r_c \delta_{m,m'} + \frac{\sin[(m - m')\Delta/2]}{\pi(m - m')} (\bar{\rho}_0 - r_c). \quad (2.15)$$

Putting Eq. (2.15) into Eq. (2.14) and then diagonalizing the H matrix, we obtain the eigenvalues $\{\lambda_j\}$ and eigenvectors of all the EM modes, from which we can calculate the resonance frequencies, induced EM dipole moments, and the polarizabilities as well as the bianisotropic polarizabilities. We will present numerical solutions of Eq. (2.13) for several examples in the following sections.

2.4.2 The Local Field Approach

The matrix problem (2.13) can be analytically solved under some reasonable assumptions, which help us to reach at an alternative approach to implement the boundary condition at the wire ends. In the limit of $\Delta \rightarrow 0$, we found from Eq. (2.15) that $\bar{\rho}(m - m') \rightarrow r_c \delta_{m,m'} + r$, where $r = \Delta \bar{\rho}_0 / 2\pi \gg r_c$ is proportional to the total resistance across the gap. We put $\bar{\rho}(m - m')$ into Eq. (2.14) and rewrite the vector-matrix equation as

$$HI = E_{\text{ext}} \quad (2.16)$$

with $H = H_0 + X$, where $H_0 = rM$, in which $M_{i,j} = 1$, and $X = \text{diag}[X_m]$ is a diagonal impedance vector-matrix with elements defined as

$$X_m = r_c + i[L_m \omega - m^2 / (\bar{C}_m \omega)]. \quad (2.17)$$

We find that the vector-matrix problem (2.16) can be analytically solved in the limit of $r \rightarrow \infty$, as follows. Now $H_0 I = 0$ so long as $\sum_m I_m = 0$. This current distribution is such that its magnitude is zero at the gap, which is a solution satisfying the desired boundary condition. However, not all I satisfying $\sum_m I_m = 0$ are the correct solutions of the circuit equation Eq. (2.13) because the internal emf inside the ring is not generally zero: $E_{\text{int}}(\phi) = \sum_m E_m \exp(im\phi) \neq 0$, where $E_m = X_m I_m - E_m^{\text{ext}}$. The only way the circuit equation Eq. (1.1) can be satisfied is if $E_{\text{int}} = \sigma \delta(\phi)$ for some constant σ ; the internal emf is zero inside the ring except at

the gap where it is counterbalanced by the infinite gap resistance r . For this to be true, it is necessary that all E_m be the same. We thus write

$$E_m = X_m I_m - E_m^{\text{ext}} = \sigma \quad (2.18)$$

so that $I_m = (E_m^{\text{ext}} + \sigma)/X_m$. The existence of these fields σ can also be appreciated from the law of charge conservation: $\partial\rho/\partial t = -\nabla \cdot \vec{j}$. At the end, the net divergence of the current \vec{j} is not zero. We thus expect localized time-varying charges and thus localized electric fields, which is represented by σ . Since $\sum_m I_m = 0$, we find the solution of σ given by:

$$\sigma = -\frac{\sum_m E_m^{\text{ext}}/X_m}{\sum_m 1/X_m} \quad (2.19)$$

The resonance frequency ω_c is determined from the condition that a nontrivial solution still exist even when $E_{\text{ext}} = 0$. We thus arrive at a sufficient resonance condition:

$$\sum_m 1/X_m(\omega_c) = 0. \quad (2.19a)$$

As we shall see, this applies to modes of even symmetry. There are additional trivial resonances of odd symmetry.

Substituting in the expression for X_m , we arrive at the equation that determines the entire spectrum:

$$1 + \sum_{m=1}^{\infty} 2(L_0\omega^2 - ir_c)/(L_m\omega^2 - m^2/\bar{C}_m - ir_c) = 0.$$

Because X_{m0} is proportional to m^2 , only a few terms in m need to be included in the above sum. We have tested the eigenfrequencies obtained from this equation with results from numerical FDTD calculations and found good agreement. Substituting in the value of the end field σ into the circuit equation, we obtain the expression for the current response to the external field:

$$I_m = (E_{\text{ext}}^m - \sum_p E_{\text{ext}}^p/X_p / \sum_n 1/X_n)/X_m. \quad (2.19b)$$

The scattered field can then be obtained from the sum $E_L(r) + E_C(r)$ for r outside of the wire.

The above consideration motivates the introduction of the boundary electric field σ . For more complicated circuit structures with free ends, it turns out to be much easier to directly deal with the boundary electric field, since it is difficult to introduce the infinite boundary resistance as we did for the split ring. Instead of imposing zero boundary current constraint directly, we introduce the idea that there is a new additional variable corresponding to a localized electric field σ at the free end of the split ring. The value of σ is chosen to satisfy the desired boundary condition—the current at the end should vanish. This boundary field is, in some

sense, like a Lagrange multiplier. The circuit equation, in terms of the Fourier component of the impedance, the external electric field E_{ext}^m and the localized electric field at the free ends, σ , is then given by

$$X_m I_m = E_{\text{ext}}^m + \sigma \quad (2.20)$$

which is consistent with Eq. (2.18). Solving Eq. (2.10) to obtain $I_m = (E_{\text{ext}}^m + \sigma) / X_m$, and then imposing the boundary condition $\sum_m I_m = 0$, we reach again at Eq. (2.19) for the solution of σ . Such consistency justifies the local field approach to implement the boundary conditions at the wire ends.

In summary, we have completed the theoretical development of the mode-expansion theory for a single-ring system, arriving at the circuit equation Eq. (2.13). This is the basic matrix equation to be solved. The circuit parameters are explicitly given in Sect. 2.3 and the boundary conditions are implemented in Sect. 2.4. In what follows, we shall apply this theory to study a single ring SRR illustrated in Fig. 2.2. For such a structure, the circuit matrix Eq. (2.13) can be analytically solved under some particular assumptions, leading to analytical results on both resonance frequencies and current distributions. Alternatively, in general situations where the analytical approach does not apply to, we can also solve Eq. (2.13) numerically to obtain all the necessary information. These two approaches are complementary to each other, and combining them significantly deepens our understandings on the inherent physics of the problem, and thus forms a comprehensive picture on the physical problem. In the following, we will separately describe the analytical and numerical approaches to study the single ring SRR.

2.5 Analytical Results for a Single Ring SRR

The circuit problem of a single ring SRR (Eq. (2.13)) can be solved analytically under the following limits: (1) $\Delta \rightarrow 0$; (2) $a/R \rightarrow 0$; (3) the metal is perfect ($r_c = 0$) and the gap is an ideal insulator ($r \rightarrow \infty$). Under these conditions, we can *rigorously* solve the vector-matrix problem which now takes the form

$$HI = 0 \quad (2.21)$$

with the Hamiltonian vector-matrix H defined in last section. The resonance frequency ω_c is determined from the condition that a nontrivial solution still exist even when $E_{\text{ext}} = 0$. We have thus set $E_{\text{ext}} = 0$ here since we only need the information of the resonance eigenmodes.

Because of the reflection (m to $-m$) symmetry of X , $X_m = X_{-m}$ there are two classes of solutions for Eq. (2.21), corresponding to even and odd symmetries under the transformation from m to $-m$. Those with odd symmetries (i.e., $I_{-m} = -I_m$) are purely geometrical resonance modes with resonance frequencies determined by $X_m = 0$. Explicitly, we found from Eq. (2.17) that the resonance frequencies are given by

$$\omega_{2m} = m\omega_u, \quad m = 1, 2, \dots \quad (2.22)$$

We note that these modes do not depend on the gap resistance r . The odd symmetry modes are simple in the limit of narrow gap $\Delta \rightarrow 0$ because the condition that $I(\phi = \Delta/2) = -I(\phi = -\Delta/2)$ implies that the current is automatically zero at the gap and there is no additional need to deal with this constraint. As the gap widens, this is no longer true. This limit can be studied with extension of the ideas described below as is described in later chapters.

To study another set of resonance modes with even symmetries (i.e., $I_{-m} = I_m$), we describe a formal approach to solve the circuit Eq. (2.21), which can be easily extended to more complicated situations. This approach explicitly displays the eigenvectors, which can be used to calculate the responses of the structures to external fields. Because r is very big, we solve the matrix problem (2.21) by a standard perturbation method. For the unperturbed matrix problem, $\mathbf{H}_0 \mathbf{I}^{(0)} = \mathbf{0}$, any vector $\mathbf{I}^{(0)}$ satisfying

$$\sum_m I_m^{(0)} = 0 \quad (2.23)$$

is a solution. Now consider the full matrix problem Eq. (2.21). Assume the solution to Eq. (2.21) can be written as $\mathbf{I} = \mathbf{I}^{(0)} + \mathbf{I}^{(1)}$, where $\mathbf{I}^{(1)}$ is of the order of $r^{-1} \mathbf{I}^{(0)}$. Put \mathbf{I} into Eq. (2.23), since $\mathbf{H}_0 \mathbf{I}^{(0)} = \mathbf{0}$, we get $\mathbf{H} \mathbf{I} = (r\mathbf{M} + \mathbf{X})(\mathbf{I}^{(0)} + \mathbf{I}^{(1)}) = r\mathbf{M}\mathbf{I}^{(1)} + \mathbf{X}\mathbf{I}^{(0)} + o(r^{-1}) = 0$. Substituting in the elements of \mathbf{X} and \mathbf{M} , we get $I_m^{(0)} = E'/X_m$ where $E' = -r \sum_{m'} I_{m'}^{(1)}$ is a constant independent of m . Employing the constrain (2.23), we arrive at the Eq. (2.19a) : $\sum_m 1/X_m = 0$, which leads to the following polynomial equation

$$1 + \sum_{m=1}^{\infty} \frac{2L_0\omega^2}{L_m\omega^2 - 1/C_m} = 0 \quad (2.24)$$

to determine the resonance frequencies. Choosing an appropriate normalization constant K , in the limit $1/r \rightarrow 0$, we find the eigenvector at resonance to be

$$\mathbf{I} = \mathbf{I}^{(0)} = K[\dots, 1/X_2, 1/X_1, 1/X_0, 1/X_1, 1/X_2, \dots]^T. \quad (2.25)$$

We emphasize that Eqs. (2.24) and (2.25) are the *exact* solutions of the matrix problem (2.21), since the perturbation theory becomes *exact* in the limit of $1/r \rightarrow 0$.

We now solve Eq. (2.24) analytically. Since as $a/R \rightarrow 0$, we have Eq. (2.12): $L_m \rightarrow \ln(R/a)$ and $1/C_m \rightarrow m^2 \ln(R/a)$, using the identity $k\pi \cot(k\pi) = 1 + \sum_{m=1}^{\infty} 2k^2/(k^2 - m^2)$ [67], we found that Eq. (2.24) can be written as $(\omega/\omega_u) \cot(\omega\pi/\omega_u) = 0$, leading to the following solutions

$$\omega_{2m+1} = (m + 1/2)\omega_u, \quad m = 0, 1, 2, \dots \quad (2.26)$$

In terms of the wavelength, this condition is equivalent to $\lambda_{2m+1} = 4\pi R/(2m+1)$.

We next study the current distribution for the resonance modes. In the thin-wire limit, we get $X_m = iL_m[\omega^2 - m^2/(L_m\bar{C}_m)]/\omega = (iL\omega_u^2/\omega)[(\omega/\omega_u)^2 - m^2]$. Therefore, according to Eq. (2.25), the current in real space is given by $I(\phi) = \sum_m e^{im\phi} I_m = K \sum_m e^{im\phi}/X_m = -iK\omega/(L\omega_u^2) \sum_m e^{im\phi}/[(\omega/\omega_u)^2 - m^2]$. Using the identity $\cos k(\phi + \pi) = k \sin k\pi[\sum_m e^{im\phi}/(k^2 - m^2)]/\pi$, we obtain, for the n th even resonance mode,

$$I(\phi) = -iK/(L\omega_u^2)\pi \sin(n+1/2)\phi. \quad (2.26a)$$

In terms of the arc length $s = R\phi$ and the circumference $l = 2\pi R$. This eigenfunction can also be written as $I(s) \propto \sin \pi s(2n+1)/l$, the same as what one expects for a straight wire. Thus, in terms of the arc length, the nature of the eigenstate does not depend much on the shape of the wire, as we discussed in Sect. 2.2.

We next discuss the response of the wire structure to external fields. The discussion in this section is general and not restricted to split rings. We shall use the notation of linear algebra so that the external electric field is written as $|E\rangle$. In Eq. (2.16) \mathbf{H} is a sum of a big (\mathbf{H}_0) and a small term (\mathbf{X}). We try to calculate the eigenstate $|f\rangle$ by perturbation theory as $|f\rangle = |w_f\rangle + |e_f\rangle$ where $H_0|w_f\rangle = 0$ and $|e_f\rangle$ is the perturbative correction. From the condition that $\mathbf{H}|f\rangle = 0$ at the resonance frequency, we obtain

$$H_0|f\rangle = H_0|e_f\rangle = -X(\omega_f)|f\rangle$$

In the language of the discussion above, $H_0|e_f\rangle = -\sigma_f$, the localized electric field at the ends for the f th eigenstate. Under an external field E and at an arbitrary frequency, we expand the current in terms of the eigenfunctions as $I = \sum_j I_f|f\rangle$ and get

$$HI \approx \sum_f I_f[H_0 + X(\omega)]|f\rangle = \sum_f I_f[X(\omega) - X(\omega_f)]|f\rangle = |E\rangle$$

We thus get

$$\sum_f I_f \langle g|[X(\omega) - X(\omega_f)]|f\rangle = \langle g|E\rangle \quad (2.27)$$

where the notation $\langle f|g\rangle = \int fg$ is used. Solving this matrix equation, we obtain the coefficients I_f .

For frequencies close to the lowest mode $|0\rangle$, we include only the term with $f = 0$ in the summation on the right hand side of the above equation. We get approximately

$$I_0 = \langle 0|E\rangle / \langle 0|[X(\omega) - X(\omega_f)]|0\rangle \quad (2.27a)$$

From these and from Eq. (2.26) the induced electric and magnetic dipole moments \mathbf{P} and \mathbf{M} induced by external electric or magnetic fields can be computed.

The information of the eigenvectors enables us to evaluate the EM responses of the system. At the n th resonance mode, from Eqs. (2.1) and (2.27), we get the current density given by $\vec{j}(r') = \vec{e}_\phi K \sin[(n + 1/2)\phi] \sin \theta \delta(\cos \theta) \delta(r' - R)/R$. The corresponding charge density is given by $\rho(r') = -i\nabla \cdot \vec{j}/\omega = -iK(n + 1/2) \cos[(n + 1/2)\phi] \sin \theta \delta(\cos \theta) \delta(r' - R)/\omega R^2$. For example, for $n = 0$, $j \propto \sin \phi/2$, $\rho \propto \cos \phi/2$, as is illustrated in Fig. 2.1

2.6 Numerical Results for a Single Ring SRR

Away from the thin-wire limit when the three conditions mentioned in Sect. 2.5 are not satisfied, the circuit equation for such systems can be solved numerically. We discuss this in this section. One main lesson we learn is that not that many Fourier modes need to be included. The convergence is very fast. This comes about because the inverse capacitance and hence the impedance X_m increases rapidly as m^2 for increasing m .

In the microwave frequency regime, we can safely set the metal's resistivity to zero (i.e., $r_c = 0$), and assume a very large but finite r for the gap resistance. We found from numerical calculations that the final results do not depend on r when $r \rightarrow \infty$. For a particular single ring SRR characterized by the wire radius a/R and the air gap size Δ , we can unambiguously compute all the circuit parameters (i.e., L_m and C_m) and thus the matrix elements $H_{m,m'}$, based on the formulas developed in Sect. 2.3. We then diagonalize the H matrix through

$$\tilde{H} = P^{-1}HP, \tilde{I} = P^{-1}I, \tilde{E}_{ext} = P^{-1}E_{ext}, \quad (2.28)$$

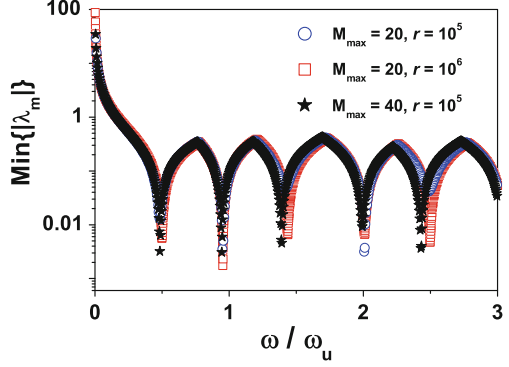
where P is the transformation matrix containing the eigenvectors of the \mathbf{H} matrix, and get from Eq. (2.13) that,

$$\tilde{I}_m = \frac{\tilde{E}_{ext}^m}{\lambda_m(\omega)} \quad (2.29)$$

where λ_m is the m th eigenvalue of the \mathbf{H} matrix. Therefore, the resonance frequencies of the system are determined by the condition $\lambda_m(\omega) \rightarrow 0$. Numerically, we determine the resonance frequencies by the condition that the magnitude of the lowest eigenvalue of the matrix H exhibits a minimum.

The magnitude of the lowest eigenvalue of matrix \mathbf{H} is shown as a function of frequency in Fig. 2.3 for a typical single ring SRR with $\Delta = \pi/40$ and $\alpha = 0.99$. The general agreements among different sets of calculations show that the adopted approximations, namely taking finite values of angular momentum cut off M_{max} and gap resistivity parameter r , do not introduce any significant errors. The series

Fig. 2.3 $\min[|\lambda_m|]$ as functions of ω/ω_u for a single-ring SRR with $\Delta = \pi/40$ and $\alpha = 0.99$, calculated with different values of M_{\max} (the cutoff value of m) and r (in units of $\mu_0\omega_u$). (From Ref. [33])



of resonances in Fig. 2.3 can be categorized into two classes. The even-numbered resonances ω_{2m} coincide well with the intrinsic resonances Ω_m , which, in consistency with the analytical results Eq. (2.22), become $\Omega_m \rightarrow m\omega_u$ in the thin-wire limit ($a/R \rightarrow 0$). Since $\lambda_{2m} = 2\pi c/\omega_{2m} = m \cdot 2\pi R$, these resonances are solely determined by the ring geometry, with currents forming standard standing waves in the ring. On the other hand, the resonance frequencies of the odd-numbered eigenmodes also match with the analytical results Eq. (2.26) very well.

The eigenvectors (contained in the matrix P defined in Eq. (2.28)) are shown in Fig. 2.4 for the lowest four resonances. The odd-numbered (even-numbered) resonance modes possess symmetrical (anti-symmetrical) eigenvectors with respect to index m , which is consistent with the analytical results. In addition, for the even-numbered modes, we note that only the $\pm m$ Fourier components are excited for the $2m$ th resonance eigenmode, verifying the analytical predictions. In contrast, for the odd-numbered modes, all Fourier components are excited but the contribution a Fourier component decrease significantly as m increases, again in agreement with the analytical results.

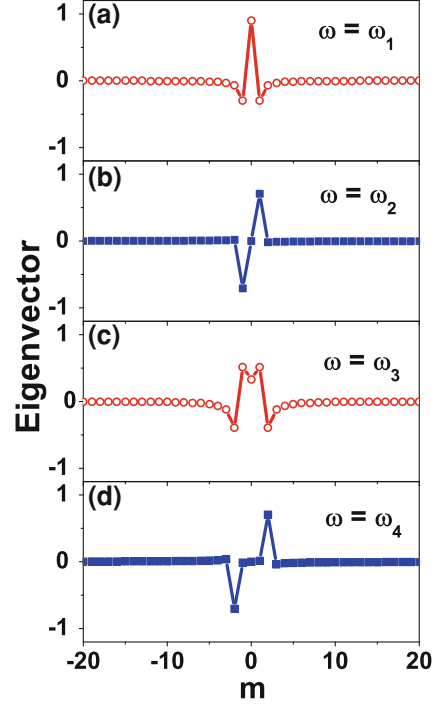
With the current distribution ($\{I_m\}$ and in turn $\vec{j}(\vec{r})$) explicitly known by diagonalizing the \mathbf{H} matrix, we can compute the electric and magnetic dipole moments \mathbf{P} and \mathbf{M} induced by external electric or magnetic fields by

$$\mathbf{M} = \frac{1}{2c} \int (\vec{r} \times \vec{j}) d\vec{r}, \mathbf{P} = \frac{i}{\omega} \int d\vec{r} (\nabla \cdot \vec{j}) \vec{r} \quad (2.30)$$

Explicitly, we find the SRR to possess the following nonzero components of dipole moments:

$$\begin{cases} p_x = \sum_j \frac{1}{\lambda_j(\omega)} \frac{\pi R}{\omega} [P_{-1j} - P_{1j}] \cdot \tilde{E}_{ext}^j \\ p_y = \sum_j \frac{1}{\lambda_j(\omega)} \frac{\pi R}{i\omega} [P_{-1j} + P_{1j}] \cdot \tilde{E}_{ext}^j \\ m_z = \sum_j \frac{\pi R^2}{\lambda_j(\omega)} P_{0j} \cdot \tilde{E}_{ext}^j \end{cases} \quad (2.31)$$

Fig. 2.4 The eigenvector distributions for the lowest eigenmode at the lowest four resonance frequencies. (From Ref. [33])



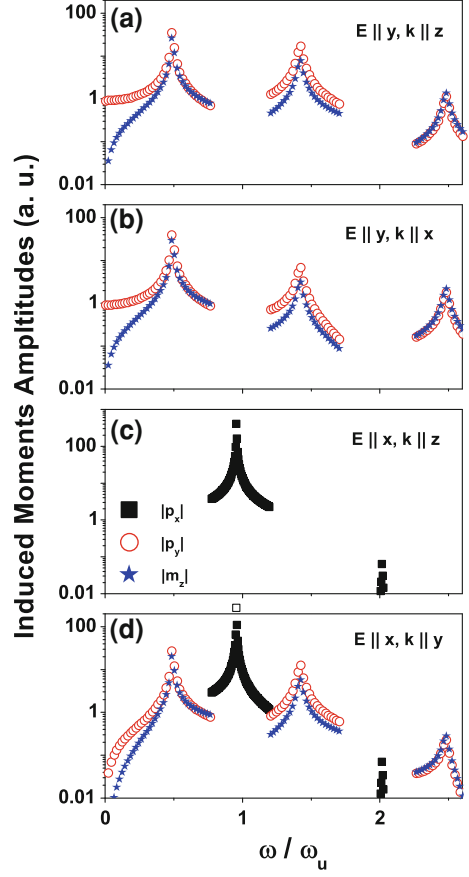
where

$$\vec{E}_{ext}^j = \sum_l (P^{-1})_{jl} E_{ext}^l = \frac{1}{2\pi} \int \sum_l (P^{-1})_{jl} \vec{E}_{ext}(\vec{r}) \cdot \vec{e}_\phi \exp(-il\phi) d\phi \quad (2.32)$$

represents the external field component projected on the j th eigenmode. A common feature of metallic wire structures is that quite often either an external magnetic or electric field alone can induce both electric and magnetic dipole moments. This property is called magnetoelectric or bianisotropic, which we will discuss explicitly in the following.

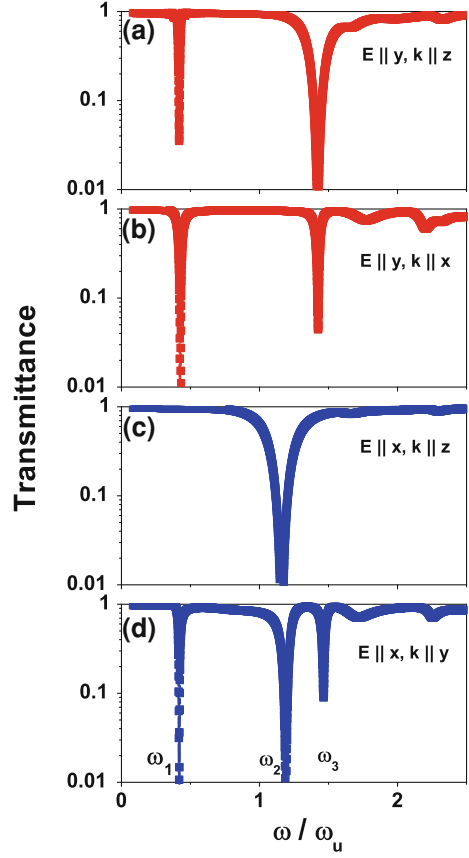
Consider different probing plane waves with (a) $\vec{E}||\hat{y}, \vec{k}||\hat{z}$, (b) $\vec{E}||\hat{y}, \vec{k}||\hat{x}$, (c) $\vec{E}||\hat{x}, \vec{k}||\hat{z}$, (d) $\vec{E}||\hat{x}, \vec{k}||\hat{y}$, we show in Fig. 2.5 the induced dipole moments as functions of the frequency. The odd-numbered resonance modes possess both magnetic (m_z) and electric (p_y) responses, while the even-numbered ones exhibit only electric (p_x) responses. The appearance of p_y is always accompanied by the appearance of m_z , which manifests the bianisotropy property of the SRR [26, 30, 32]. Symmetry restricts a probing field to excite only a particular set of resonance modes of the SRR, and therefore, not all the resonance peaks appear simultaneously in each spectrum. We have performed FDTD simulations [66] to verify these theoretical results. To model a single ring SRR with $R = 4\text{mm}$, $a = 0.1\text{mm}$, and $\Delta = \pi/40$,

Fig. 2.5 Amplitudes of the induced moments, $|p_x|$, $|p_y|$, $|m_z|$, of the SRR as functions of ω/ω_u for different probing fields as shown in the figure. (From Ref. [33])



we first construct a 0.2 mm-thick metallic disk of radius 4.1 mm, then cut it by a 0.2 mm-thick air disk of radius 3.9 mm, and finally cut an air gap of the required width on the resulting structure. It is difficult to employ FDTD simulations to directly compute the dipole moments of a single SRR induced by an external plane wave. Instead, we study the transmission spectrum of an array of such SRR's, and identify the resonances by the dips of the transmission spectrum. For the two configurations studied in Fig. 2.5a, c, we construct SRR arrays to periodically tile the xy -plane, with lattice constants 16 mm along both x and y directions. For the other two configurations, we construct SRR arrays to periodically tile the xz - or yz - plane, respectively, with a lattice constant = 12 mm along x or y direction and 16 mm along z direction. The transmission spectra under the four plane wave inputs are shown, respectively in Fig. 2.6 a–d. When we compare Fig. 2.6 with the results shown in Fig. 2.5, we find that they agree with each other quite well. We clearly identify the dips at $\omega \approx 0.42\omega_0$ shown in Fig. 2.6a–d as the lowest eigen resonance mode (ω_1), the dips at $\omega \approx 1.19\omega_0$ shown in Fig. 2.6c, d as the second resonance mode (ω_2), and the dips at

Fig. 2.6 FDTD calculated transmission spectra of the SRR arrays as functions of ω/ω_u for plane wave inputs specified in the figure. Here the SRR has $R = 4$ mm, $a = 0.1$ mm, and $\Delta = \pi/40$. (From Ref. [32])



$\omega \approx 1.46\omega_0$ as the third one (ω_3). The quantitative differences between analytical and FDTD results must be caused by the couplings among different SRRs, since we have to adopt periodic arrays of SRRs to study the transmission spectra in the FDTD simulations.

2.7 Summary

In this chapter, we have established a rigorous mode-expansion theory for metallic systems in ring geometry in which the inductive/capacitive effects were included completely and the relevant circuit parameters were calculated rigorously. We have applied the theory to study the EM resonance properties of a single ring SRR. We found that the circuit problem can be analytically solved for ideal structures, leading to several useful analytical formulas for both resonance frequencies and current distributions. For general nonideal structures, we numerically solved the

circuit equation and found that the obtained results match well with FDTD simulations on realistic structures. While there have been lots of efforts to study the SRRs theoretically, we believe an analytical theory established on more rigorous grounds is highly desirable, particularly since it can yield more physical insight and analytical formulas helpful for researchers working in this area.

Appendix

We describe the evaluation of the circuit elements in this Appendix. The current is along the ring, in component form, it is $j = (-\sin \varphi, \cos \varphi, 0)|j|$. We expand the current in a Fourier series as $|j| = \sum_m j_m \exp(im\varphi)$. We get $j_- = j_x - ij_y = \sum_m j_m \exp[i(m+1)\varphi]$.

In the QSA, the Green's function is proportional to $1/|r - r'| = 4\pi/(2l+1) \sum r_{<}^l Y_{lm}(\Omega) Y_{lm}^*(\Omega')/r_{>}^{l+1}$. We take the coordinate system so that the z axis is perpendicular to the ring. The ring is thus in the plane with $\theta=0$. Assume a time dependence of the form $\exp(i\omega t)$. For the self inductance of a single ring, the expansion parameter is $\alpha = r_{<}/r_{>} = (R-a)/R$ where a is the radius of the wire that makes up the ring. For the mutual inductance of two concentric rings, the expansion parameter is $r_{<}/r_{>} = R_1/R_2$. Carrying out the integration for $E_L^m = -i\omega \sum_m L_{mm'} I_{m'} L_{mm'} = \frac{1}{2\pi} \iint (\hat{e}_\phi \cdot \hat{e}_{\phi'}) e^{i(m'\phi' - m\phi)} g(\phi, \phi') R d\phi' d\phi / c^2$ we get, using the definition of the spherical harmonics $Y_{lm} = [(2l+1)(l-m)!/4\pi(l+m)!]^{1/2} P_l^m(\cos \theta) e^{im\phi}$,

$$E_{m-1} = -i\omega/c^2 \sum_l [P_l^m(0)]^2 [(l-m)!/(l+m)!] j_{m-1} \alpha^l / R \quad (\text{A.1})$$

The inductance is thus given by

$$L_{m-1} = \sum_{l=m}^{\infty} A_l(m) \alpha^l / (Rc^2) \quad (\text{A.1a})$$

where

$$A_l(m) = [P_l^m(0)]^2 [(l-m)!/(l+m)!]. \quad (\text{A.2})$$

We show below that for large l ,

$$A_l(m) \approx \pi^{-1} l^{-1} 2. \quad (\text{A.3})$$

This slow decrease of the coefficients $A_l(m)$ of the infinite series with respect to l leads to a log dependence on $1-\alpha$. We thus get

$$L_{m-1} = [B_{m-1} + \log(R/2b)/\pi] / (Rc^2) \quad (\text{A.4})$$

with a nonlog dependent coefficient B_m .

Asymptotic Behavior of $A_l(m)$

We now examine the asymptotic behavior of the coefficient of the infinite series. Now the associated Legendre polynomial at the origin is given by [68] $P_l^m(0) = 2^m \pi^{-1/2} \cos[\pi(l+m)/2] \Gamma((l+m+1)/2) / \Gamma[(l-m)/2 + 1]$. The asymptotic behavior of the Gamma function for large n is given by $\Gamma(n) \propto \exp(-n)n^{n-1/2}$. We get $P_l^m(0) = 2^m \pi^{-1/2} \cos[\pi(l+m)/2] R$ where the ratio of the Gamma functions is given by $R = \exp(-m+1/2) [(l+m+1)/2]^{(l+m+1)/2} / [(l-m)/2 + 1]^{(l-m)/2+1}$. R can be written as $R = (l/2)^{m-1/2} \exp[-m+1/2 + [(l+m+1) \ln(1 + (m+1)/l)/2 - (l-m+2) \ln[1 + (2-m)/l]]/2]$. In the large l limit we get $P_l^m(0) \approx \pi^{-1/2} \cos[\pi(l+m)/2] l^{m-1/2} 2^{1/2} \exp[-m+1/2 + (m+1)/2 - (2-m)/2]$. This can be simplified as

$$P_l^m(0) \approx \pi^{-1/2} \cos[\pi(l+m)/2] l^{m-1/2} 2^{1/2}. \quad (\text{A.5})$$

We thus have $A_m(l) \approx [P_l^m(0)]^2 \exp[2m + (l-m+1/2) \ln(1 + (1-m)/l) - (l+m+1/2) \ln(1 + (1+m)/l)] l^{-2m}$. In the large l limit, this becomes

$$A_m(l) \approx [P_l^m(0)]^2 \exp[2m + (1-m) - (1+m)] l^{-2m}. \quad (\text{A.6})$$

Substituting in Eq. (A.5), we get Eq. (A.3).

Numerical Evaluation

The inductances can be calculated recursively. $P_l^m(0) = 2^m \pi^{-1/2} \cos[\pi(l+m)/2] \Gamma((l+m+1)/2) / \Gamma[(l-m)/2 + 1]$. $P_m^m(0) = 2^m \pi^{-1/2} \cos(\pi m) \Gamma(m+1/2) / \Gamma(1) = 2^m \pi^{-1/2} (-1)^m [(1)(3) \dots (2m-1)] \pi^{1/2} / 2^m$. $A_m(m) = P_m^m(0)^2 / (2m)! = [(1)(3) \dots (2m-1)]^2 / (2m)!$.

$$A_m(m) = (1)(3) \dots (2m-1) / [(2m)(2m-2) \dots 2].$$

$$P_{l+2}^m(0) = -P_l^m(0)(l+m+1)/(l-m+2).$$

$$A_{l+2}(m) = A_l(m)(l+m+1)^2 [(l+2-m)(l+1-m)] / [(l+2+m)(l+1+m)] (l-m+2)^2.$$

$$A_{l+2}(m) = A_l(m) [(l+m+1)(l+1-m)] / [(l+2+m)(l-m+2)].$$

Beyond QSA

It is possible to include the effect of the radiation resistance by using the formula $\exp(ik|r - r'|)/|r - r'| = 4\pi ik \sum_l j_l(kr_<) h_l(kr_>) \sum_m Y_{lm}(\Omega) Y_{lm}^*(\Omega')$.

Instead of Eq. (2.1a) we now have

$$L_{m-1} = \sum_{l=m}^{\infty} A_l(m) j_l(k|R - a|) h_l(kR) / (Rc^2) \quad (\text{A.7})$$

The formula for $A_l(m)$, Eq. (A.2) and its asymptotic form, Eq. (A.3) remains the same.

The leading correction to the QSA result is a damping term proportional to kR . This can also be seen trivially from the formula $\exp(ik|r - r'|)/|r - r'| \approx 1/|r - r'| + ik$.

This calculation can be easily generalized to the mutual inductance of two separate but concentric rings.

References

1. V.G. Veselago, Sov. Phys. Usp. **10**, 509 (1968)
2. L. Landau, E.M. Lifschitz, *Electrodynamics of Continuous Media* (Elsevier, New York, 1984)
3. J.B. Pendry, A.J. Holden, D.J. Robbins, W.J. Stewart, IEEE Trans. Microwave Theory Tech. **47**, 2075 (1999)
4. D.R. Smith, W.J. Padilla, D.C. Vier, S.C. Nemat-Nasser, S. Schultz, Phys. Rev. Lett. **84**, 4184 (2000)
5. R.A. Shelby, D.R. Smith, S. Schultz, Science **292**, 77 (2001)
6. H.O. Moser, B.D.F. Casse, O. Wilhelmi, B.T. Saw, Phys. Rev. Lett. **94**, 063901 (2005)
7. G. Dolling, M. Wegener, C.M. Soukoulis, S. Linden, Opt. Lett. **32**, 53 (2007)
8. G. Dolling, C. Enkrich, M. Wegener, C.M. Soukoulis, S. Linden, Opt. Lett. **31**, 1800 (2006)
9. S. Zhang, W. Fan, N.C. Panoiu, K.J. Malloy, R.M. Osgood, S.R.J. Brueck, Phys. Rev. Lett. **95**, 137404 (2005)
10. V.M. Shalaev, W. Cai, U.K. Chettiar, H. Yuan, A.K. Sarychev, V.P. Drachev, A.V. Kildishev, Opt. Lett. **30**, 3356 (2005)
11. J.B. Pendry, Phys. Rev. Lett. **85**, 3966 (2000)
12. N. Fang, H. Lee, C. Sun, X. Zhang, Science **308**, 534 (2005)
13. A. Ono, J. Kato, S. Kawata, Phys. Rev. Lett. **95**, 267407 (2005)
14. P.A. Belov, Y. Hao, S. Sudhakaran, Phys. Rev. B **73**, 033108 (2006)
15. N. Engheta, IEEE Antennas Wireless Propag. Lett. **1**, 10 (2002)
16. L. Zhou, H. Q. Li, Y. Q. Qin, Z. Y. Wei, and C. T. Chan, Appl. Phys. Lett. **86**, 101101 (2005)
17. H. Li, J. Hao, L. Zhou, Z. Wei, L. Gong, H. Chen, C. T. Chan, Appl. Phys. Lett. **89**, 104101 (2006)
18. I. Gil, J. Garcia-Garcia, J. Bonache, F. Martin, M. Sorolla, R. Marques, Electron. Lett. **40**, 1347 (2004)
19. K. Aydin¹, I. Bulu¹, K. Guven¹, M. Kafesaki, C. M Soukoulis, and E. Ozbay, New J. Phys. **7**, 168 (2005).
20. A. Radkovskaya, M. Shamonin, C.J. Stevens, G. Faulkner, D.J. Edwards, E. Shamonina, L. Solymar, Microwave Opt. Technol. Lett. **46**, 473 (2005)

21. K.A. Boulais, D.W. Rule, S. Simmons, F. Santiago, V. Gehman, K. Long, A. Rayms-Keller, *Appl. Phys. Lett.* **93**, 043518 (2008)
22. K. Aydin, E. Ozbay, J. Appl. Phys. **101**, 024911 (2007)
23. K. Aydin, K. Guven, N. Katsarakis, C.M. Soukoulis, E. Ozbay, *Opt. Express* **12**, 5896 (2004)
24. B. Sauviac, C.R. Simovski, S.A. Tretyakov, *Electromagnetics* **24**, 317 (2004)
25. M. Shamonin, E. Shamonina, V. Kalinin, L. Solymar, *J. Appl. Phys.* **95**, 3778 (2004)
26. R. Marqués, F. Mesa, J. Martel, F. Medina, *IEEE Trans. Antennas Propag.* **51**, 2572 (2003)
27. F. Aznar, J. Bonache, F. Martin, *Appl. Phys. Lett.* **92**, 043512 (2008)
28. V. Zhurbenko, T. Jensen, V. Krozer, P. Meincke, *Microwave Opt. Technol. Lett.* **50**, 511 (2008)
29. M. Shamonin, E. Shamonina, V. Kalinin, L. Solymar, *Microwave Opt. Technol. Lett.* **44**, 133 (2005)
30. J. García-García, F. Martín, J.D. Baena, R. Marqués, L. Jelinek, *J. Appl. Phys.* **98**, 033103 (2005)
31. J.D. Baena, R. Marques, F. Medina, J. Martel, *Phys. Rev. B* **69**, 014402 (2004)
32. R. Marques, F. Medina, R. Rafii-El-Idrissi, *Phys. Rev. B* **65**, 144440 (2002)
33. L. Zhou, S.T. Chui, *Phys. Rev. B* **74**, 035419 (2006)
34. L. Zhou, S.T. Chui, *Appl. Phys. Lett.* **90**, 041903 (2007)
35. X.Q. Huang, Y. Zhang, S.T. Chui, L. Zhou, *Phys. Rev. B* **77**, 235105 (2008)
36. S.T. Chui, Y. Zhang, L. Zhou, *J. Appl. Phys.* **104**, 034305 (2008)
37. N. Katsarakis, T. Koschny, M. Kafesaki, E.N. Economou, C.M. Soukoulis, *Appl. Phys. Lett.* **84**, 2943 (2004)
38. P. Markos, C.M. Soukoulis, *Phys. Rev. E* **65**, 036622 (2002)
39. J. Zhou, Th Koschny, M. Kafesaki, E.N. Economou, J.B. Pendry, C.M. Soukoulis, *Phys. Rev. Lett.* **95**, 223902 (2005)
40. T.J. Yen, W.J. Padilla, N. Fang, D.C. Vier, D.R. Smith, J.B. Pendry, D.N. Basov, X. Zhang, *Science* **303**, 1494 (2004)
41. S. Linden, C. Enkrich, M.n Wegener, J. Zhou, T. Koschny, C. M. Soukoulis, *Science* **306**, 1351 (2004)
42. J. Zhou, T. Koschny, C.M. Soukoulis, *Opt. Express* **15**, 17881 (2007)
43. M.W. Klein, C. Enkrich, M. Wegener, C.M. Soukoulis, S. Linden, *Opt. Lett.* **31**, 1259 (2006)
44. E.N. Economou, Th Koschny, C.M. Soukoulis, *Phys. Rev. B* **77**, 092401 (2008)
45. Q. Zhao, L. Kang, B. Du, B. Li, J. Zhou, H. Tang, X. Liang, B. Zhang, *Appl. Phys. Lett.* **90**, 011112 (2007)
46. C. Enkrich, M. Wegener, S. Linden, S. Burger, L. Zschiedrich, F. Schmidt, J.F. Zhou, Th Koschny, C.M. Soukoulis, *Phys. Rev. Lett.* **95**, 203901 (2005)
47. F. Bilotti, A. Toscano, L. Vegni, *IEEE Trans. Antennas Propag.* **55**, 2258 (2007)
48. A.K. Azad, A.J. Taylor, E. Smirnova, J.F. O'Hara, *Appl. Phys. Lett.* **92**, 011119 (2008)
49. D.R. Smith, D.C. Vier, N. Kroll, S. Schultz, *Appl. Phys. Lett.* **77**, 2246 (2000)
50. D.R. Smith, S. Schultz, P. Markos, C.M. Soukoulis, *Phys. Rev. B* **65**, 195104 (2002)
51. B. Popa, S.A. Cummer, *Phys. Rev. B* **72**, 165102 (2005)
52. K.B. Alicia, E. Ozbay, *J. Appl. Phys.* **101**, 083104 (2007)
53. B.E. Little, S.T. Chu, H.A. Haus, J. Foresi, J.-P. Laine, *J. Lightwave Technol.* **15**, 998 (1997)
54. R. Marques, J. Martel, F. Mesa, F. Medina, *Phys. Rev. Lett.* **89**, 183901 (2002)
55. H. Xu, Z. Wang, J. Hao, J. Dai, L. Ran, J.A. Kong, L. Zhou, *Appl. Phys. Lett.* **92**, 041122 (2008)
56. M.C.K. Wiltshire, J.B. Pendry, I.R. Young, D.J. Larkman, D.J. Gilderdale, J.V. Hajnal, *Science* **291**, 849 (2001)
57. M.C.K. Wiltshire, J.V. Hajnal, J.B. Pendry, D.J. Edwards, C.J. Stevens, *Opt. Express* **11**, 709 (2003)
58. E. Verney, B. Sauviaca, C.R. Simovski, *Phys. Lett. A* **331**, 244 (2004)
59. J.D. Baena, L. Jelinek, R. Marqués, J. Zehentner, *Appl. Phys. Lett.* **88**, 134108 (2006)
60. J.D. Baena, L. Jelinek, R. Marqués, J.J. Mock, J. Gollub, D.R. Smith, *Appl. Phys. Lett.* **91**, 191105 (2007)

61. J.D. Baena, L. Jelinek, R. Marqués, Phys. Rev. B **76**, 245115 (2007)
62. P. Gay-Balmaz, O.J.F. Martin, Appl. Phys. Lett. **81**, 939 (2002)
63. Q. Zhao, L. Kang, B. Du, H. Zhao, Q. Xie, X. Huang, B. Li, J. Zhou, L. Li, Phys. Rev. Lett. **101**, 027402 (2008)
64. Th Koschny, L. Zhang, C.M. Soukoulis, Phys. Rev. B **71**, 121103 (2005)
65. J.D. Jackson, *Classical Electromagnetic*, 3rd edn. (Wiley, New York, 1999)
66. CONCERTO 4.0, Vector Fields Limited, England, 2005
67. See, for example, Matthews and Walker, Mathematical Physics, Benjamin, New York, 1965, pp. 50–51, Eq. (2.33)
68. Handbook of Mathematical functions by Abramowitz and Stegun Eq. (8.6.1)

Electromagnetic Behaviour of Metallic Wire Structures

Chui, S.T.; Zhou, L.

2013, X, 142 p., Hardcover

ISBN: 978-1-4471-4158-7